

Prediction of broadband noise from rotating blade elements with serrated trailing edges

F

Cite as: Phys. Fluids **34**, 085109 (2022); <https://doi.org/10.1063/5.0094423>

Submitted: 03 April 2022 • Accepted: 14 July 2022 • Published Online: 08 August 2022

 Haopeng Tian (田浩朋) and  Benshuai Lyu (吕本帅)

COLLECTIONS

F

This paper was selected as Featured



[View Online](#)



[Export Citation](#)



[CrossMark](#)

ARTICLES YOU MAY BE INTERESTED IN

Toward high-efficiency low-noise propellers: A numerical and experimental study
Physics of Fluids **34**, 076116 (2022); <https://doi.org/10.1063/5.0098891>

Aeroacoustic investigation of asymmetric oblique trailing-edge serrations enlightened by owl wings

Physics of Fluids **34**, 015113 (2022); <https://doi.org/10.1063/5.0076272>

Aeroacoustic interaction between owl-inspired trailing-edge fringes and leading-edge serrations

Physics of Fluids **34**, 011907 (2022); <https://doi.org/10.1063/5.0078974>



Physics of Fluids

Special Topic: Paint and Coating Physics

Submit Today!

Prediction of broadband noise from rotating blade elements with serrated trailing edges

Cite as: Phys. Fluids 34, 085109 (2022); doi: 10.1063/5.0094423

Submitted: 3 April 2022 · Accepted: 14 July 2022 ·

Published Online: 8 August 2022



Haopeng Tian (田浩朋)^{1,2}  and Benshuai Lyu (吕本帅)^{1,2,a)} 

AFFILIATIONS

¹State Key Laboratory for Turbulence and Complex Systems, Department of Aeronautics and Astronautics, College of Engineering, Peking University, Beijing 100871, People's Republic of China

²Joint Laboratory of Marine Hydrodynamics and Ocean Engineering, Pilot National Laboratory for Marine Science and Technology (Qingdao), Shangdong 266237, People's Republic of China

^{a)}Author to whom correspondence should be addressed: b.lyu@pku.edu.cn

ABSTRACT

This paper conducts a theoretical investigation into the prediction of broadband trailing-edge noise for rotating serrated blades. Lyu's semi-analytical noise prediction model for isolated flat plates is extended to rotating blades using Schlinker and Amiet's approach and applied to three test applications including a wind turbine, a cooling fan, and an open propeller. The model is validated by comparing the straight edge results with that presented in the work of Sinayoko *et al.*, which shows an excellent agreement. The noise spectra obtained using different-order approximations show that the second-order solution yields a converged result. It is found that trailing-edge serrations can lead to noise reduction in the intermediate- and high-frequency ranges at an observer angle of 45° at low Mach numbers but may lead to noise increase in the intermediate-frequency range at high Mach numbers. The results show that the directivity patterns change due to the use of trailing-edge serrations and the directivity peaks are observed at high frequencies. A detailed analysis on the effects of rotation shows that for low-Mach number applications, the Doppler effect is weak and the peaky directivity pattern is mainly affected by the nonuniform directivity of an isolated flat plate at high frequencies. However, for high-Mach number applications, the Doppler effect is significant and also contributes to the final directivity pattern of rotating blades.

Published under an exclusive license by AIP Publishing. <https://doi.org/10.1063/5.0094423>

I. INTRODUCTION

Noise emission is an important issue in many applications concerning rotating blades, such as wind turbines, cooling fans, and unmanned aerial vehicles (UAVs) with propellers. There exist several different noise generation mechanisms for an airfoil encountering a uniform flow.¹ Among these mechanisms, trailing-edge (TE) noise has attracted significant attention in the past few decades. TE noise is produced via the scattering of a turbulent boundary layer by the sharp trailing edge of an airfoil and is believed to be the dominant noise source for wind turbine blades.² In addition, TE noise is found to be one of the major noise sources for the broadband noise produced by the blades of UAVs.³

For an isolated flat plate in a uniform flow, Amiet⁴ developed an analytical model to predict the far-field noise produced by the turbulent flow past a trailing edge. In Amiet's flat plate model, the Schwarzschild method was used to solve the convective wave equation. The far-field noise spectral density was calculated from the wavenumber spectral density of the wall surface pressure. The model was

subsequently extended to investigate the noise from rotor blades,^{5,6} where the blade was divided into several segments. For each segment, it was assumed that the rotation motion could be viewed as translational within an infinitesimal time interval. Consequently, in each time interval, the prediction model for isolated flat plate may be used. The final noise prediction result is the weighted average over the angular position, with the weighting factor being related to the Doppler effect.⁶ Combining this theoretical model and suitable experimental measurements, Schlinker and Amiet⁶ found that TE noise from a full-scale helicopter main rotor plays an important role in the total broadband noise spectrum at high frequencies. In recent years, Schlinker and Amiet's approach for rotating blades was validated both analytically and experimentally.^{7–9} As pointed by Schlinker and Amiet,⁶ direct measurements of the flow parameters beneath the boundary layer near the trailing edge were needed as inputs to the accurate prediction of noise. Rozenberg *et al.*⁸ conducted unsteady wall-pressure measurements by inserting small microphones into industrial ventilation fan blades. These results were used in the analytical model which was an

extension of Schlinker and Amiet's formulas including the back-scattering correction proposed by Roger and Moreau.¹⁰ Good agreement was observed between the far-field measurements and model predictions at most observer angles. A new formulation for TE noise radiation from the rotating blade based on an analytical solution of the convective wave equation was proposed by Sinayoko *et al.*⁹ This was compared to the Schlinker and Amiet's theory for the rotating blade and shown to be applicable to both low- and high-speed applications.

Inspired by the silent flight of owls,^{11–14} trailing-edge serrations were used as a promising approach to reduce TE noise. In 1991, Howe developed an analytical model to study the noise reduction effect of a serrated trailing edge on a semi-infinite plate.^{15,16} The prediction model showed that sharp sawtooth serrations could lead to better performance than sinusoidal serrations. However, later experiments found that Howe's model significantly overpredicted the noise reduction capability of trailing-edge serrations.^{17,18} The possible reason for the discrepancy was later identified to be the inaccurate Green's function used in Howe's model. Recently, Lyu *et al.*¹⁸ proposed an analytical noise prediction model based on Fourier expansion and Schwarzschild technique. In Lyu's model, the convective wave equation was transformed into a set of coupled partial differential equations, which were solved by an iterative procedure. This new model shows much more realistic predictions than Howe's model. It was also shown that the physical mechanism for noise reduction is the destructive interference effects of the wall pressure fluctuations caused by the serrated trailing edge. Based on the Wiener-Hopf method, Huang¹⁹ and Ayton²⁰ proposed two analytical models for noise prediction from serrated trailing edges. In addition to the theoretical approach, a number of numerical and experimental studies concerning the noise reduction effect of serrated trailing edges have been carried out.^{21–30} For example, the direct numerical simulations conducted by Jones and Sandberg^{21,22} showed that the serrations had little impact on the directivity and spanwise coherence of the trailing-edge noise, and changes in the noise radiation are more likely due to changes to the scattering process itself. Chong and Vathylakis²⁵ experimentally investigated the velocity and thermal properties of the turbulent boundary layer on a serrated sawtooth surface. They found that the variations of wall pressure power spectral density and spanwise coherence in a sawtooth trailing edge play a minor role in the reduction of self-noise. Moreau and Doolan²⁶ conducted an experimental study and showed that wide serrations provide greater noise reduction than narrow ones, which is contrary to theoretical predictions. They concluded that, for the particular configuration they used, the noise reduction is due to the influence of serrations on the hydrodynamic field at the source location. A very recent review of turbulent boundary layer trailing-edge noise in theoretical, computational, and experimental aspects can be found from Lee *et al.*³¹

While the noise reduction by isolated flat plates or airfoils with serrated trailing edges has received much attention, research on the rotating blade case is still at its early stage. Such problems are of practical interest in many applications. For example, the experiments conducted by Oerlemans *et al.*² used full-scale wind turbine blades to show that a 3.2 dB overall noise reduction was obtained for blades with serrated trailing edges. UAVs used extensively in civil and military fields is another area of significant interest. Many experimental investigations have confirmed the noise reduction effects of trailing edge serrations on UAV propellers.^{32–40} Ning *et al.*³⁷ experimentally

investigated the performance of UAV propellers with different sawtooth serrations. It was found that a 0.9–1.6 dB noise reduction was achieved. The experiments by Lee *et al.*³⁵ showed that a half flat tip serrated blade could lead to more noise reduction than the quarter flat tip and rectangular serrated propellers. Compared with numerical and experimental approaches, analytical models are much more robust and less resource demanding. However, analytical noise prediction models for rotating blades with serrated trailing edges are still rare. Sinayoko *et al.*⁴¹ developed a model that combined Howe's isolated airfoil model with Amiet's rotating blade method and studied the effects of three different types of serrations. It is worth noting that Lyu's model was also extended to the rotating blade in Sinayoko's work, but only the zeroth-order (decoupled) solution was used. Following the same idea, Halimi *et al.*⁴² investigated the noise reduction effects of a small remotely piloted aircrafts (RPAs) propeller with sawtooth serrations using the first-order approximation. Yet, as mentioned by Halimi *et al.*,⁴² "the implementation of the second-order approximation is necessary to assess its influence on the predicted spectra." In addition, it is unknown that how the serrations perform in various operating conditions, such as that in wind turbines, cooling fans, etc.

The aim of the present work is to develop a second-order accurate model to predict far-field noise and examine the effects of serration on noise reduction for rotating blades in various operating conditions. Lyu's model for isolated flat plates and Schlinker and Amiet's approach for rotating blades are combined and applied to three different typical applications. The performance of zeroth-, first-, and second-order solutions is compared and the effects of rotation are discussed. The reason why we use Lyu's model rather than Ayton's, in particular, the simplified model by Lyu and Ayton,⁴³ is that the latter model is strictly two dimensional. That is to say, the span is infinitely long and the boundary layer extends to infinity in the spanwise direction, and therefore, the resulting noise is of a cylindrical nature. Therefore, the magnitude of the scattered pressure would decay as $1/\sqrt{r}$, where r is the cylindrical radius. In practice, the observer nearly always located in the far-field, and the interested blade segment (such as the blade tip of a wind turbine) has a finite span. When the distance is large, the produced sound field inevitably becomes three dimensional, and the magnitude of the scattered pressure decays with $1/r$, where r denotes the observer distance in a spherical coordinates. In applications with rotating blades, the distance between the noise source and the observer is varying during the rotation process; therefore, a 3D-accurate model must be used to account for this. As the transition from a near-field two-dimensional to a far-field three-dimensional sound is gradual, it is not straightforward to extend Ayton's model to the rotating case, and we, therefore, use Lyu's model instead. This paper is organized as follows. Section II briefly outlines the derivation of the far-field noise prediction model developed by Lyu *et al.* and the Schlinker and Amiet's approach for rotating blades. Sound spectra and directivity patterns using the second-order solution are presented in Sec. III together with discussions about the effects of rotation. Section IV summarizes and concludes the present paper.

II. TRAILING-EDGE NOISE PREDICTION MODEL FOR ROTATING BLADE ELEMENTS

When a blade rotates, the spanwise flow field is not uniform. It is rational to divide the blade into several elements and the overall noise

is calculated by summing the noise radiated from all blade elements. It is widely known, however, significant noise emission occurs near the blade tip, where the instantaneous rotation speed is large. Furthermore, the present work aims to understand the effects of rotation on the noise reduction performance of serrations. It suffices, therefore, in this paper to study the noise reduction of one blade element.

A. Noise prediction model for an isolated flat plate with the serrated trailing edge

Consider a thin flat plate with the serrated trailing edge (Fig. 1), whose average chord length is c and spanwise length is d . The root-to-tip amplitude and wavelength of the sawtooth serraion are $2h$ and λ , respectively. In the coordinate frame of this problem, the streamwise, spanwise, and normal to the plate coordinates are X , Y , and Z , respectively. The observer point is located at (X_0, Y_0, Z_0) .

When turbulence is scattered at the trailing edge, the total pressure can be decomposed into two parts, i.e., the incident wall pressure and the scattered pressure. The latter satisfies the convective wave equation

$$\nabla^2 p - \frac{1}{c_0^2} \left(\frac{\partial}{\partial t} + U \frac{\partial}{\partial X} \right)^2 p = 0, \quad (1)$$

where p is the scattered pressure, t is the time, and c_0 and U denote the speed of sound and the uniform flow speed in the streamwise direction, respectively. Suppose that the pressure perturbation is harmonic, namely, $p = P(X, Y, Z)e^{-i\omega t}$, where ω is the angular frequency. The far-field sound pressure can be found to be¹⁸

$$p_f(\mathbf{X}, \omega) = \left(\frac{-i\omega Z_0 c}{4\pi c_0 S_0^2} \right) \int_{-\infty}^{\infty} \lambda \times \frac{\sin((N + 1/2)\lambda(k_2 - kY_0/S_0))}{\sin((k_2 - kY_0/S_0)\lambda/2)} \times \mathcal{L}(\omega, \bar{k}_1, k_2) P_i(\omega, k_2) dk_2, \quad (2)$$

where $k = \omega/c_0$, $\bar{k}_1 = \omega/U_c$, U_c denotes the convection velocity of the wall pressure gusts, $S_0^2 = X_0^2 + \beta^2(Y_0^2 + Z_0^2)$, $\beta^2 = 1 - M_0^2$, $M_0 = U/c_0$, k_2 is the spanwise wavenumber, $2N + 1$ represents the number of sawteeth on the edge, and P_i is the magnitude of the incident wall pressure gust. \mathcal{L} is the gust-response function whose detailed form is given by

$$\mathcal{L}(\omega, \bar{k}_1, k_2) = (1 - i) \frac{1}{\lambda c} e^{-ik(M_0 X_0 - S_0)/\beta^2} e^{ik(M_0 - X_0/S_0)h/\beta^2} \times \sum_{n'=-\infty}^{\infty} (\Theta_{n'} + \Theta_{n'}^{(1)} + \Theta_{n'}^{(2)} + \dots). \quad (3)$$

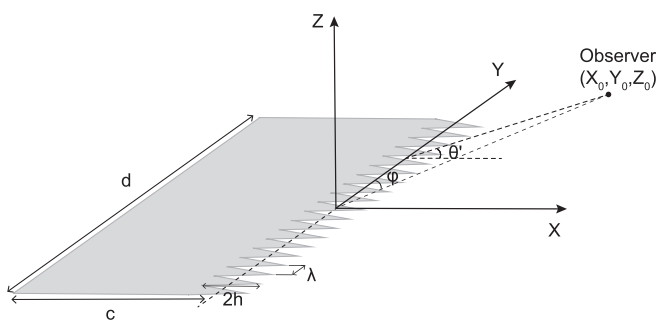


FIG. 1. Schematic of a flat plate with trailing-edge serrations.

The definition of $\Theta_{n'}$, $\Theta_{n'}^{(1)}$, and $\Theta_{n'}^{(2)}$ and more details about the derivation can be found from the work of Lyu *et al.*¹⁸ The power spectral density (PSD) of the far-field sound can be approximated by

$$S_{pp}(\mathbf{X}, \omega) = \left(\frac{\omega Z_0 c}{4\pi c_0 S_0^2} \right)^2 2\pi d \times \sum_{m=-\infty}^{\infty} |\mathcal{L}(\omega, \bar{k}_1, 2m\pi/\lambda + kY_0/S_0)|^2 \times \Pi(\omega, 2m\pi/\lambda + kY_0/S_0). \quad (4)$$

Here, Π denotes the wavenumber spectral density of the hypothetical wall pressure fluctuations beneath the turbulent boundary layer near the edge.

B. Schlinker and Amiet's model for the rotating blade

As shown in Fig. 2, consider a rotating blade element with the serrated trailing edge and pitch angle α in a uniform flow of Mach M_{FO} . The angular velocity of the blade element is constant and the blade Mach number is M_{BO} . The observer is stationary relative to the hub. Following the Schlinker and Amiet's approach,⁶ the rotating movement can be viewed as translational in an infinitesimal time interval. Sinayoko *et al.*⁹ presented a detailed derivation of the theory for baseline blades. To facilitate easy comparison, we follow the same notation here.

When the blade element rotates by an angle γ (see Fig. 2), consider a pulse of sound emitted by the sound source on the blade element. When the sound wave reaches the observer, the sound source has moved to a new position \mathbf{x}_p and the propagation time is denoted by T_e (see Fig. 3). For the observer \mathbf{x}_o in the far field, the sound source may be assumed to be located at the hub. Thus, the convected source position can be approximated by

$$\mathbf{x}_c \approx c_0 T_e \mathbf{M}_{FO}. \quad (5)$$

The distance between the convected source position and the observer equals to the propagation time multiplied by the speed of sound, i.e.,

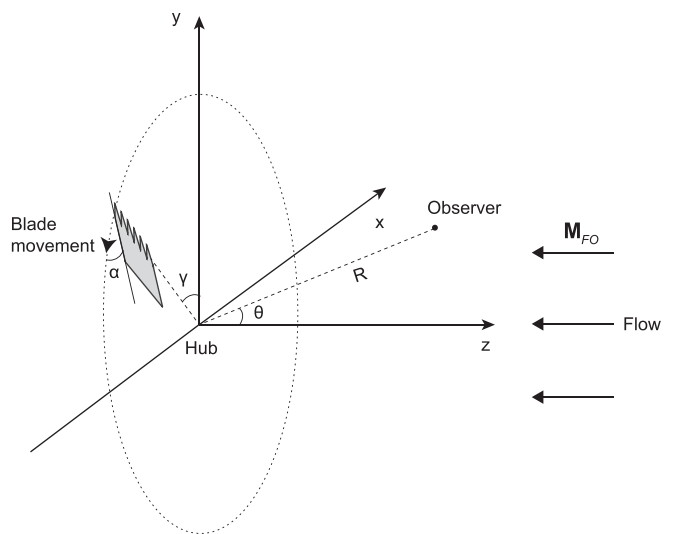


FIG. 2. Schematic of a rotating blade element with the serrated trailing edge.

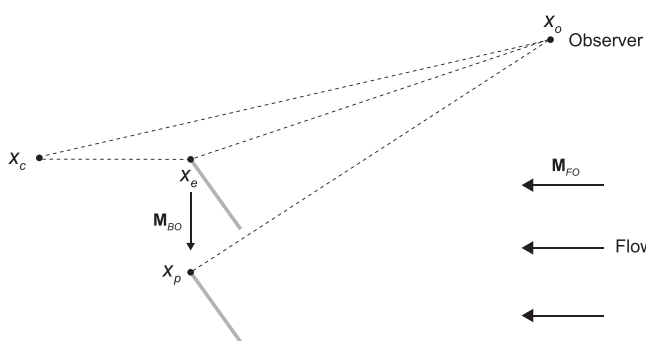


FIG. 3. Emission position, present position, and convected position of a noise source.

$$|\mathbf{x}_o - \mathbf{x}_c| = c_0 T_e. \quad (6)$$

Substituting Eq. (5) into Eq. (6), we can obtain a second-order polynomial equation

$$|\mathbf{x}_o - c_0 T_e \mathbf{M}_{FO}|^2 \approx (c_0 T_e)^2. \quad (7)$$

The propagation time T_e can be solved from Eq. (7). Similarly, the present position when the sound wave reaches the observer can be approximated by

$$\mathbf{x}_p \approx \mathbf{M}_{BO} c_0 T_e. \quad (8)$$

To make use of the noise prediction theory for an isolated flat plate, the coordinate system needs to be transformed to be the one where the airfoil remains fixed while the observer moves accordingly. The first step of the coordinate transformation is to move the origin of the coordinate system to the present source position \mathbf{x}_p , i.e.,

$$\mathbf{x}_1 = \mathbf{x}_o - \mathbf{x}_p. \quad (9)$$

Then, as showed in Fig. 4(a), rotate the \mathbf{x}_1 -coordinate system counter-clockwise by an angle γ around the z_1 -axis, i.e.,

$$\mathbf{x}_2 = A_1(\gamma) \mathbf{x}_1, \quad (10)$$

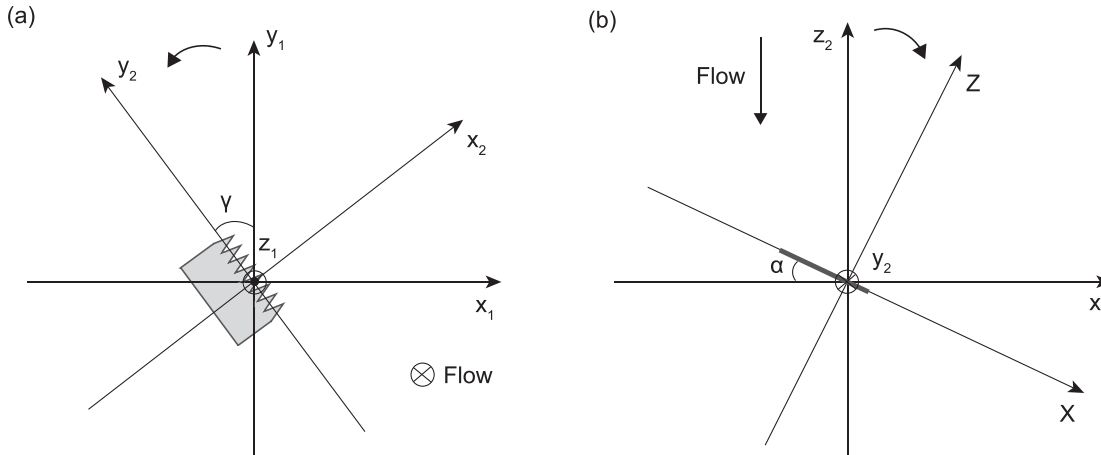


FIG. 4. Coordinate rotation: (a) in the x_1-y_1 plane by the angle of γ and (b) in the x_2-z_2 plane by the angle of α .

where A_1 is the rotation matrix in the x_1-y_1 plane whose definition can be found in Appendix A. The final coordinate system $\mathbf{X} = (X, Y, Z)$ is obtained by rotating the \mathbf{x}_2 -coordinate system clockwise by an angle α around the y_2 -axis

$$\mathbf{X} = A_2(\alpha) \mathbf{x}_2, \quad (11)$$

where A_2 is the rotation matrix in the x_2-z_2 plane whose definition can also be found in Appendix A.

The frequency received by the observer ω is related to the instantaneous emitted frequency ω' through the Doppler shift⁴⁴

$$\frac{\omega}{\omega'} = 1 + \frac{\mathbf{M}_{BO} \cdot \widehat{\mathbf{CO}}}{1 + (\mathbf{M}_{FO} - \mathbf{M}_{BO}) \cdot \widehat{\mathbf{CO}}}, \quad (12)$$

where $\widehat{\mathbf{CO}}$ denotes the unit vector from the convected source position to the observer position. The instantaneous sound PSD of the rotating blade element is given by

$$S_{pp}(\mathbf{x}_o, \omega, \gamma) = \frac{\omega'}{\omega} S'_{pp}(\mathbf{X}, \omega', \gamma), \quad (13)$$

where S'_{pp} can be calculated using Eq. (4). The time-averaged PSD is obtained by averaging Eq. (13) over one rotation of the rotor. Thus, the integral over the rotation angle $0 \leq \gamma < 2\pi$ can be written as

$$\bar{S}_{pp}(\mathbf{x}_o, \omega) = \frac{1}{2\pi} \int_0^{2\pi} \left(\frac{\omega'}{\omega} \right)^2 S'_{pp}(\mathbf{X}, \omega', \gamma) d\gamma, \quad (14)$$

where, as demonstrated by Sinayoko *et al.*,⁹ the correct exponent of the Doppler term should be 2. Equation (14) is the fundamental equation of this paper. Substituting Eq. (4) into Eq. (14), we can evaluate the noise spectra emitted from the rotating blade for arbitrary observer locations.

III. RESULTS AND DISCUSSION

In this section, we apply this serrated noise prediction model to three different applications, i.e., a wind turbine, a cooling fan, and an open-propeller and discuss the effects of rotation on the noise

TABLE I. Parameters of the applications considered.

	Wind turbine	Cooling fan	Open propeller
Radius	21.75 m	0.30 m	1.35 m
Chord	2 m	0.13 m	0.31 m
α	10°	34°	17° (takeoff), 38° (cruise)
M_{BO}	0.165	0.0525	0.748
M_{FO}	0.029	0.0354	0.229 (takeoff), 0.584 (cruise)
Re_c	7.5×10^6	1.8×10^5	5.4×10^6 (takeoff), 6.6×10^6 (cruise)

reduction of serrations in each operating condition. Note both takeoff and cruise operating conditions are considered in the last application. These applications cover a wide range of Mach numbers and have been used in the studies of Blandeau and Joseph⁷ and Sinayoko *et al.*⁹

Table I lists the main parameters of these applications, where Re_c is the Reynolds number based on the chord c . As can be expected, the Reynolds number for the cooling fan is the smallest among the three applications due to the small Mach numbers and the short chord. The Reynolds numbers for the wind turbine and the open propeller are close. However, as will be shown in the following analysis, the noise reduction effects are quite different for these two applications. This is mostly due to the significant difference in their Mach numbers, as can be seen from **Table I**. Similar to previous studies,⁹ the far-field noise generated by one blade element at zero angle of attack is discussed. The spanwise length of the element is set to be a third of the radius of the blade.

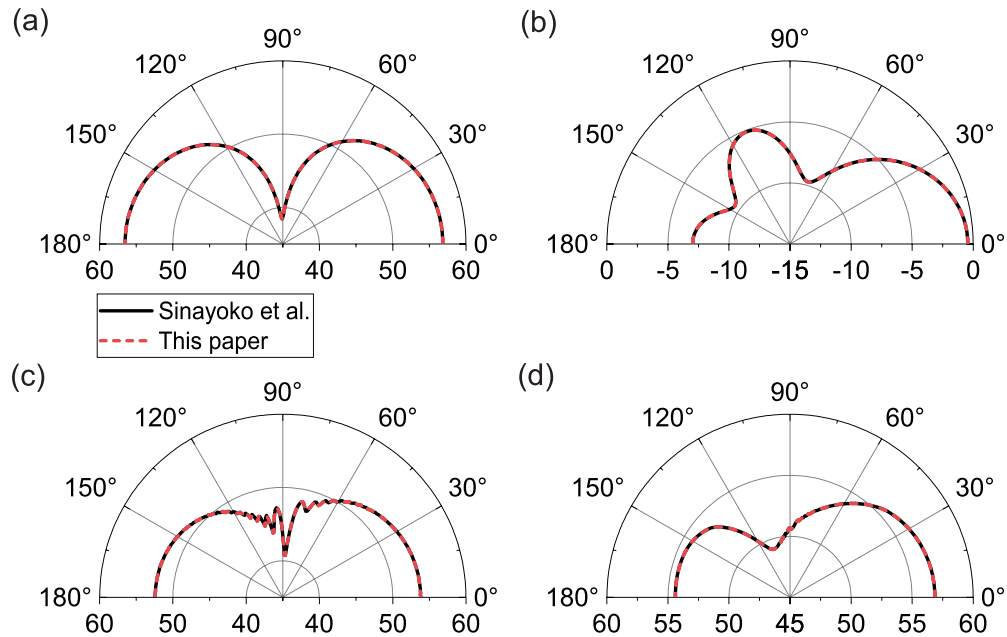


FIG. 5. Comparison of the directivity patterns for rotating blade elements with straight trailing edges using the model presented in this paper and that presented in the work of Sinayoko *et al.*⁹ (a) Wind turbine, $kc = 0.5$; (b) cooling fan, $kc = 5$; (c) open propeller at takeoff, $kc = 50$; and (d) open propeller at cruise, $kc = 50$.

A. Validation

It is known that Lyu's model reduces to Amiet's model when the serration's amplitude reduces to zero. Consequently, the result obtained using the present model should reduce to the baseline (straight trailing edge) rotation model based on Amiet's approach when h approaches 0. To validate this new model, the far-field directivity patterns for baseline rotating blade elements using Lyu's model are compared with the results presented in the work of Sinayoko *et al.*,⁹ where Amiet's model is used. All three orders of solutions are used and yield the same result. The wall pressure model of Chou and George⁴⁵ is used in the validation (see **Appendix B**). **Figure 5** shows a comparison of the directivity patterns for rotating blade elements between the present model and that in Sinayoko *et al.*⁹ The Sound Pressure Level (SPL) is calculated as follows:

$$SPL(f) = 10 \log_{10} \left(\frac{2\pi S_{pp}(\omega)}{P_{ref}^2} \right), \quad (15)$$

where $P_{ref} = 2 \times 10^{-5}$ Pa. The factor 2π is due to the definition of Fourier transform used in Lyu's work. Amiet's model for flat plate is presented in **Appendix B** for reference. It is worth noting that the linear interpolation process of the acoustic lift in the study of Sinayoko *et al.*⁹ is neglected here.

As showed in **Fig. 5**, excellent agreement is observed for all three applications listed in **Table I**. Three chosen normalized frequencies are $kc = 0.5$, $kc = 5$, and $kc = 50$ for the wind turbine, cooling fan, and open propeller, respectively. For the open propeller, both the takeoff and cruise conditions are shown [**Figs. 5(c)** and **5(d)**, respectively]. Since the straight trailing edge can be viewed as a special case of the serrated trailing edge when the amplitude of the serration is

sufficiently small, this excellent agreement demonstrates the correct formulation of the present model.

B. Second-order solution

Using this validated model, we are in a position to use the second-order solution to assess the effects of rotation on the noise reduction of serrations in all three applications. As the first step, we study the predicted spectra of three applications using zeroth-, first-, and second-order approximations, respectively, to examine the convergence of each iteration. Chase's turbulent boundary layer spectrum model^{16,46} is used to calculate $\Pi(\omega, k_2)$ to be

$$\Pi(\omega, k_2) \approx \frac{4C_m \rho^2 v_*^4 (\omega/U_c)^2 \delta^4}{U_c ((\omega/U_c)^2 + k_2^2) \delta^2 + \chi^2}, \quad (16)$$

where $C_m \approx 0.1553$, $\chi \approx 1.33$, $v_* \approx 0.03U$, ρ is the density of the fluid, and δ is the turbulent boundary layer thickness, which is approximated by⁴⁷

$$\delta/c = 0.382 Re_c^{-1/5}. \quad (17)$$

Since sharp sawtooth serrations result in greater noise reduction,^{15,16} λ/h is set to 0.4. As shown in Fig. 6, without loss of generality, the observer point is set to be located at the x - z plane and the initial position of the blade element is set on the positive y -axis in the following studies.

Figure 7 shows the far-field sound spectra for all four operating conditions using different order solutions. The observer angle is 45° and the noise spectra are calculated at a large observer distance of 1000 m, but rescaled to 1 m for visualization. It can be shown that similar to the results for the isolated flat plate, the discrepancy between first- and second-order approximations is relatively small compared with that between zeroth- and first-order approximations, showing that the second-order approximation yields a converged accurate solution. As shown in Figs. 7(a) and 7(b), significant noise reduction is achieved in the intermediate- and high-frequency range for wind turbines and cooling fans. However, noise increases are observed in the intermediate-frequency range for open propellers [Figs. 7(c) and 7(d)] due to the use of serrations. This is likely because the effective Mach

number that the blade element sees is considerably high (approximately 0.8 for takeoff and 0.95 for cruise) in these two cases. The wetted length of the trailing edge may be longer than that of a straight one, and the destructive interference of the scattered surface pressure caused by serrations is relatively weak. Such a phenomenon was also observed in the experiments of Cambray *et al.*³² for a UAV propeller rotating at high speeds. At high frequencies, the noise reduction effect appears to be significant again.

The applications considered in this paper include wind turbines, cooling fans, and open-propellers, whose typical operating conditions are proposed by Blandeau and Joseph.⁷ In what follows, we compare the model predictions with relevant experimental results on the performance of rotating blades with serrated trailing edges used on UAV propellers and wind turbines. Recently, Yang *et al.*⁴⁰ carried out an experimental study using multi-copter rotors with serrated trailing edges during forward flight. Six sets of sawtooth serrations with different shapes were installed on the test rotor in the retrofitted manners of add-on and cut-in. The experimental results by Yang *et al.* showed that significant noise reduction was observed in the intermediate frequency range for both cut-in and add-on serrations, which is consistent with the prediction results. Noise increase at high frequencies is slightly more pronounced in the add-on cases. This phenomenon is similar to that observed in the experiments on wind turbines. The noise prediction agrees with the measurement for both cut-in and add-on trailing-edge serrations, but with minor deviations for the add-on case at high frequencies, which is possibly due to the change in the flow and turbulence statistics. From an acoustic scattering point of view, whether using add-on or cut-in serrat would not make too much difference. However, it is another story for the flow. The turbulence statistical properties of the boundary layer may be significantly different between these two scenarios. We believe that the slight noise increase observed for the add-on case is likely caused by a change in the flow statistics, in particular, the wavenumber–frequency spectrum of the pressure fluctuations beneath the turbulent boundary layer. Noise reduction effects at intermediate and high frequencies can also be found in several cases of the experimental investigations on UAV propellers of Lee *et al.*,³⁵ Li *et al.*,⁴⁸ and Ning *et al.*³⁷ In particular, both the model predictions in the present paper and the experimental results of Cambray *et al.*,³² Li *et al.*,⁴⁸ and Lee *et al.*³⁵ indicate that trailing-edge serrations may be less effective for propellers operating at high speeds. It is worth noting that the practical noise reduction performance of trailing-edge serrations is related to a variety of factors, including shapes, sizes, angles of attack, retrofitted manners, rotating speeds, observer angles, etc. Thus, the trends discussed here are operating-condition dependent. For wind turbines, Mathew *et al.*⁴⁹ conducted field tests of trailing-edge serrations installed on a 120 m turbine (blade diameter). The noise spectra at a wind turbine speed of 9 m/s showed that serrations were effective in reducing noise in the intermediate-frequency range (100–1000 Hz), which is consistent with the model prediction. At higher frequencies, the increase in noise levels due to the use of serrations was observed. The field test results of Braun *et al.*,⁵⁰ Lee and Lee,⁵¹ and Oerlemans⁵² exhibited similar trends. The noise increase occurred at high frequency is likely due to the change in the flow physics, such as a cross-flow through the valleys of the sawtooth, especially for blades at high angles of attack.¹⁷

Because the wavenumber–frequency spectrum is not available in most practical experiments, it is rather difficult to make a quantitative

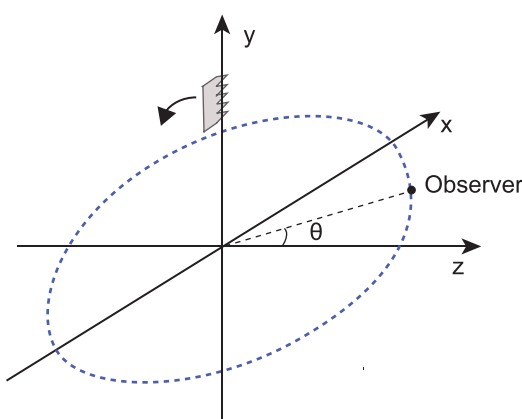


FIG. 6. The location of the observer and the initial position of the blade element.

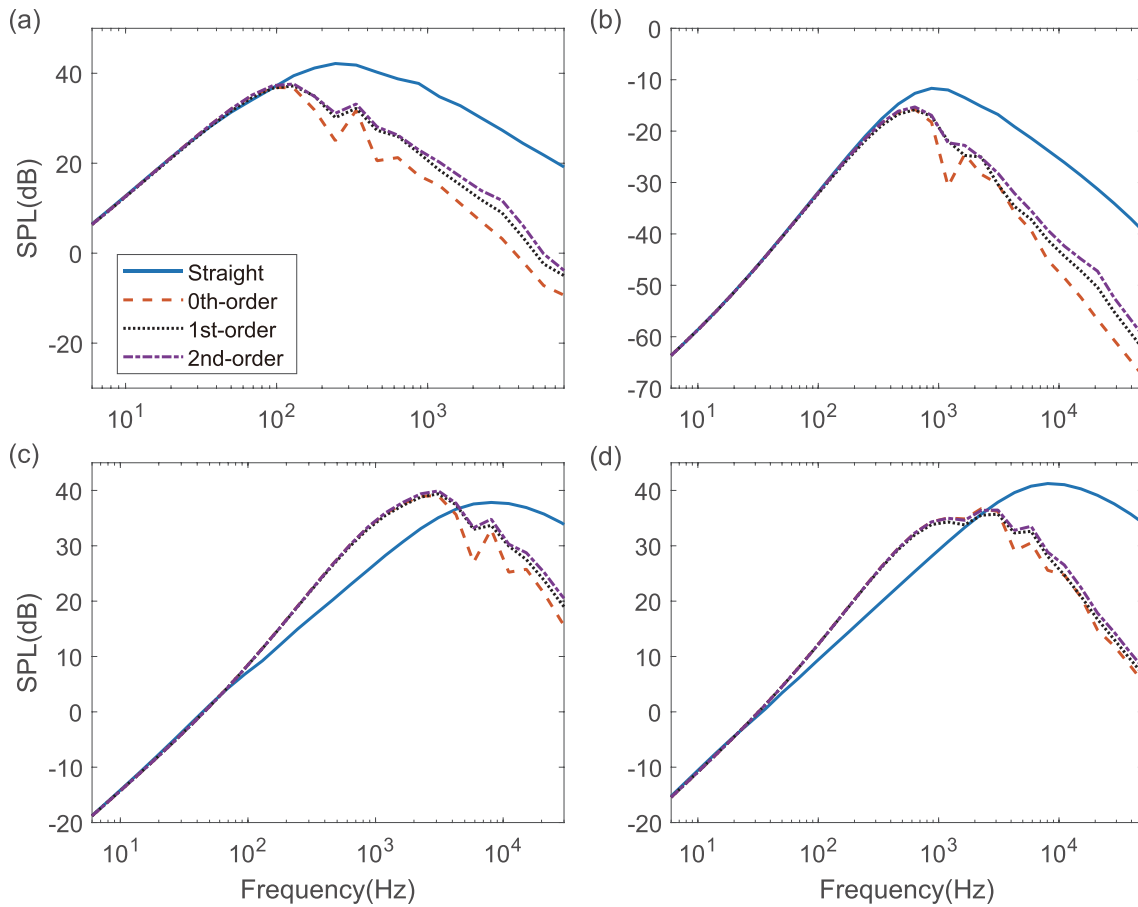


FIG. 7. The trailing-edge noise SPL at $\theta = 45^\circ$: (a) wind turbine, (b) cooling fan, (c) open propeller at takeoff, and (d) open propeller at cruise.

comparison with experimental data. The present model uses Chase's model for a flat plate as its input. However, it is well-known that in practical applications, the wavenumber–frequency spectrum would be significantly different from that of a flat plate. Recognizing that quantitative agreement is likely not to be achieved, we try to make a qualitative comparison of the noise reduction between the prediction and experiments. Figure 8 shows the comparison of the noise reduction between the theoretical prediction and experimental measurements using full-scale turbine blades by Oerlemans *et al.*² The measurement condition used for comparison is state 2a defined in Oerlemans *et al.*² and the incoming flow velocity is 10 m/s. The length of the serrations is 20% of the chord length and λ/h is estimated to be around 0.4. The noise reduction ΔSPL is defined as the difference between the SPL for the baseline and serrated models. It can be seen that a noise reduction of up to 5 dB is observed in the frequency range of 100–2000 Hz. The model can give a good prediction when the frequency is less than 500 Hz. As the frequency increases, the model starts to give overpredictions. This kind of overprediction is common in trailing-edge noise models for isolated airfoils.^{17,29} It is widely believed that such overprediction is caused by two possible reasons. The first is the inaccuracy of the wavenumber–frequency spectrum. Chase's model is used in the prediction model. Chase's model is an empirical wavenumber–frequency spectrum model

describing the surface pressure statistics within a turbulent boundary layer over a flat plate. However, in the experiments, the turbine blades have both thickness and camber and are placed at nonzero angle of attack. The characteristics of the boundary layer must be different from that for a flat plate. It is, therefore, likely to introduce significant errors, especially at high frequencies. The second reason is connected with the new flow physics that might occur in the flow. It is known experimentally¹⁷ that when airfoils with serrated edges are under loading, microjets would appear within the serration teeth. Such new flow features could become new noise sources that affect the noise reduction performance of serrations, especially at high frequencies. Nevertheless, considering that we use a highly idealized wavenumber–frequency spectrum in the model and neglect the effects of new flow features, the prediction at low frequencies can be regarded satisfactory.

C. Directivity patterns under different operating conditions

Figures 9 and 10 present the SPL directivity patterns for the three applications in the x - z plane at three normalized frequencies, i.e., $kc = 0.5, 5$, and 50 . The distance between the observer and the hub is again rescaled to 1 m and the flow direction is from right to left.

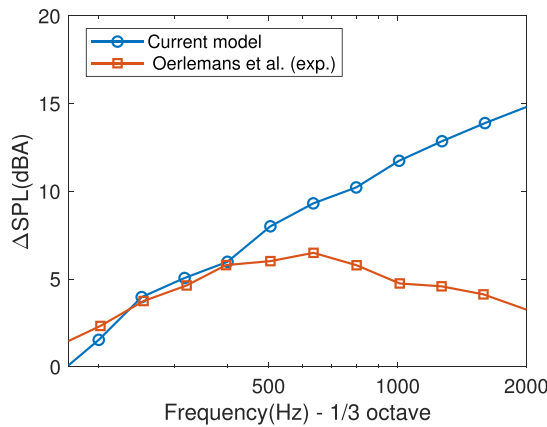


FIG. 8. Comparison of the noise reduction between the theoretical prediction and experimental measurements using full-scale wind turbine blade.²

Second-order solution is used in the far-field PSD calculation. For the blade element of wind turbines, as shown in Fig. 9(a), there exists no obvious noise reduction at low frequency. At intermediate frequency, i.e., $kc = 5$, the effects of serrations vary with observer angles [Fig. 9(c)]. The sound pressure level for the serrated trailing edge is lower than the baseline in the range $30^\circ < \theta < 140^\circ$. However, noise enhancement is observed at remaining observer angles, i.e., the noise level is slightly higher in the position just before and behind the rotation plane due to the use of serrations. On the other hand, significant noise reduction can be seen in all directions when $kc = 50$ [Fig. 9(e)]. Figures 9(b), 9(d), and 9(f) show that the serrated trailing edge can lead to noise reduction for all observer angles for the cooling fan blades. From Fig. 10, we can see that for the propeller blade, noise reduction appears mainly at high frequencies for both takeoff and cruise conditions. In addition, the noise reduction effect of the serrated trailing edge is more significant in the observer angle range $0^\circ < \theta < 30^\circ$ at $kc = 5$ and in $0^\circ < \theta < 60^\circ$ at $kc = 50$ under the cruise condition [Figs. 10(d) and 10(f)]. Noise increase may occur at lower frequencies, which is consistent with the results in Figs. 7(c) and 7(d).

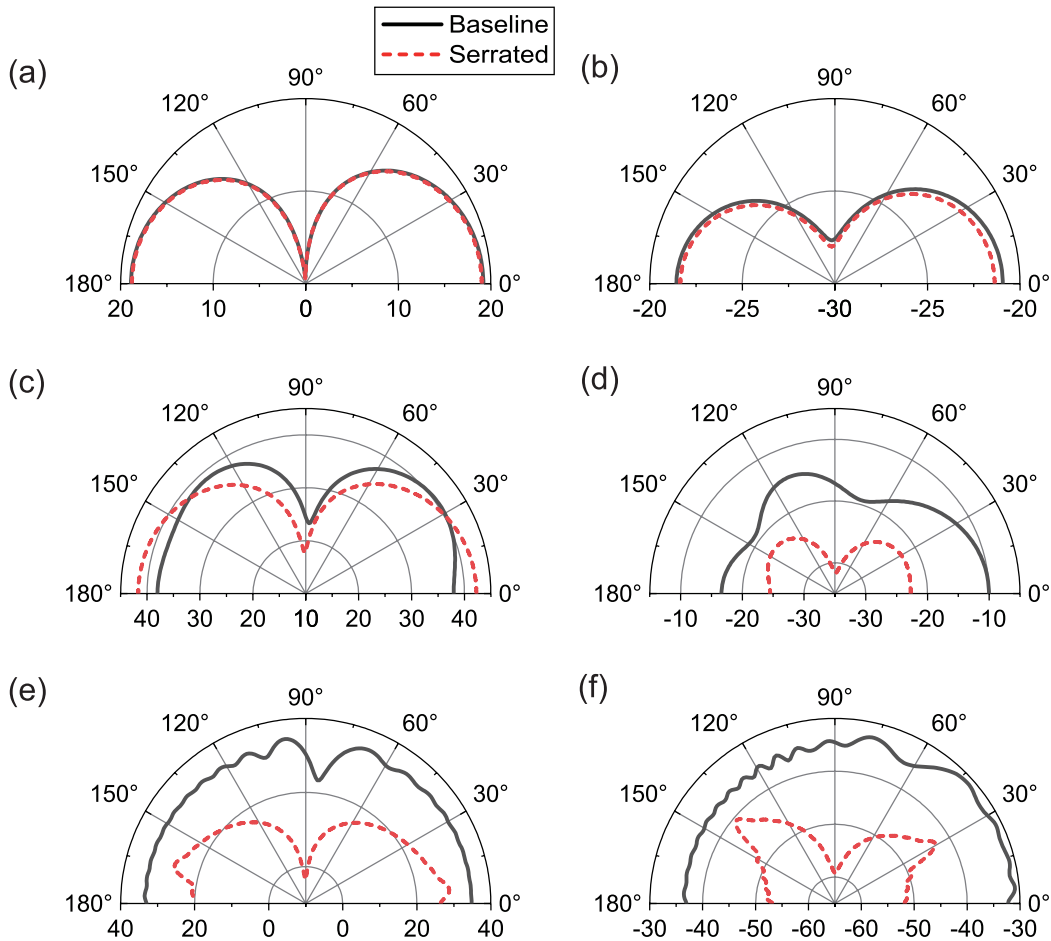


FIG. 9. SPL directivities for rotating blade elements with straight and serrated trailing edges: (a) wind turbine, $kc = 0.5$; (b) cooling fan, $kc = 0.5$; (c) wind turbine, $kc = 5$; (d) cooling fan, $kc = 5$; (e) wind turbine, $kc = 50$; and (f) cooling fan, $kc = 50$.

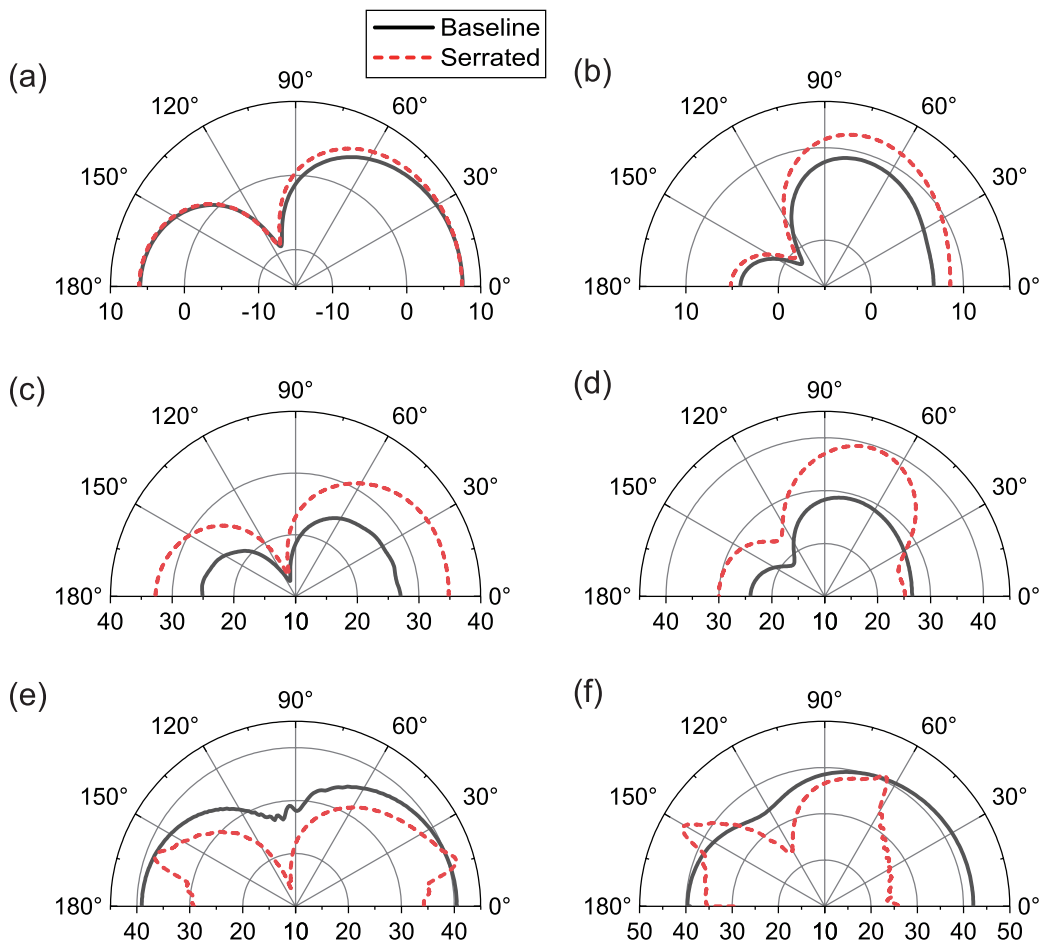


FIG. 10. SPL directivities for rotating blade elements with straight and serrated trailing edges: (a) open propeller at takeoff, $kc = 0.5$; (b) open propeller at cruise, $kc = 0.5$; (c) open propeller at takeoff, $kc = 5$; (d) open propeller at cruise, $kc = 5$; (e) open propeller at takeoff, $kc = 50$; and (f) open propeller at cruise, $kc = 50$.

It is interesting to note that at the normalized frequency $kc = 50$, there exist several peaks in the directivity patterns under four operating conditions, for example, at 30° and 140° for the cooling fan and at 60° and 150° for the open propeller (at cruise). Section III D will attempt to explain this. In summary, trailing-edge serrations in rotating blade elements can result in either significant noise reduction or non-negligible noise increase depending on the blade Mach number and frequency; noise increase is more likely to occur at high Mach numbers in the intermediate frequency regime. The shapes of the directivity pattern can also undergo pronounced distortions compared with those baseline case.

D. Discussion on the effects of rotation

In this section, we discuss the effects of rotation on the far-field noise generated by rotating blade elements with serrated trailing edges.

1. Doppler effect

In the Schlinker and Amiet's approach for rotating blades, a coordinate transformation is performed to make use of the theoretical

model developed for isolated airfoils. For an observer point not located on the z -axis, the distance between the noise source and the observer is constantly changing during a rotation cycle. The relative velocity between the sound source and the observer depends on the instantaneous location of the blade, so does the Doppler frequency shift. The Doppler shift, defined in Eq. (12), can be calculated explicitly to be

$$\frac{\omega}{\omega'} = \frac{\sqrt{1 - M_{FO}^2 \sin^2 \theta}}{\sqrt{1 - M_{FO}^2 \sin^2 \theta + M_{BO} \cos \gamma \sin \theta}}. \quad (18)$$

In deriving Eq. (18), we assume the source to be located on the hub.

Figure 11 shows the Doppler shift (ω/ω') vs the rotation angle γ at a number of different observer angles (θ). From Eq. (18), we can see that the value of the Doppler shift is symmetric about the x - y plane, so only the results within the observer angle range 0° – 90° are presented here. When the observer point is located on the z -axis, i.e., the observer angle $\theta = 0^\circ$, the distance between the blade element and the observer is constant during the rotating process. Consequently, no Doppler effect appears, and the Doppler shift equals to 1 for all

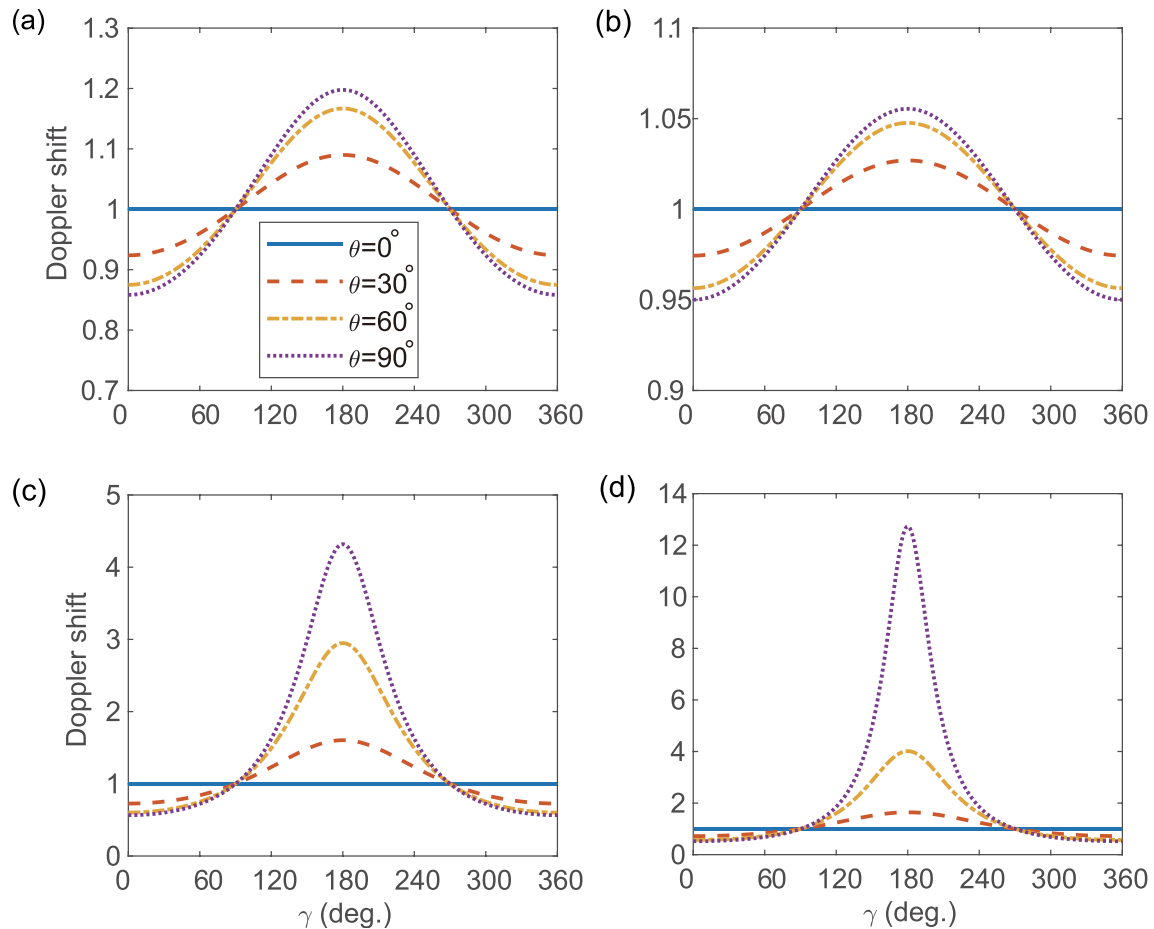


FIG. 11. Variation of the Doppler shift with the rotation angle γ at different observer angles θ . (a) Wind turbine, (b) cooling fan, (c) open propeller at takeoff, and (d) open propeller at cruise.

rotation angles as shown in Fig. 11. For a fixed nonzero value of θ , it can be seen that the maximal and minimal values occur when $\gamma = 180^\circ$ and 0° , respectively. This is because the relative velocity between the blade element and the observer attains a maximal value in these cases. As the observer angle increases, the Doppler effect becomes significant and reaches the maximum at $\theta = 90^\circ$, i.e., the observer is in the rotation plane. It is shown in Figs. 11(a) and 11(b) that the Doppler shift is close to 1, which indicates that the Doppler effect is relatively weak for wind turbines and cooling fans, especially the latter. This is not surprising, given the small values of Mach numbers involved in these two applications. However, for the open propeller at takeoff and cruise, the Doppler effect is significant due to the higher Mach numbers as shown in Figs. 11(c) and 11(d). It is known experimentally that the noise from wind turbine blades is most significant when the blade rotates downwards approaching the microphone arrays placed on the ground.² In Fig. 11, we show that the Doppler effect is not significant for wind turbines and cooling fans. The large SPL variations as the blade rotates to different angles may, therefore, be due to the highly nonuniform noise directivity of an isolated blade (as shown below). This can be used to partly explain the highest noise

emission when the blade is rotating toward the microphone array used in the experiment.²

2. The effects of averaging

In the reference frame fixed on the blade, the blade is static while the observer is considered to be moving. The noise levels at different observer locations are, therefore, varying. The results shown in Figs. 7, 9, and 10 represent an average of these values. To show the instantaneous variation of the perceived sound when the blade rotates to different angles, we show, in Figs. 12 and 13, the perceived SPL by the observer at 200 rotation angles for all the frequencies of interest. The observer is located in the x - z plane and the observer angle is 45° . Also shown is the averaged result, it is clear that the curve of time-averaged spectra denoted by the black line appears in the middle of the shaded area, which is formed by the instantaneous spectra curves at various rotation angles. As shown in Fig. 12, the instantaneous SPL variations for straight trailing edges are approximately within 5–15 dB in a rotation. However, it can be seen from Fig. 13 that the variations are much larger for serrated trailing edges, especially at high frequencies.

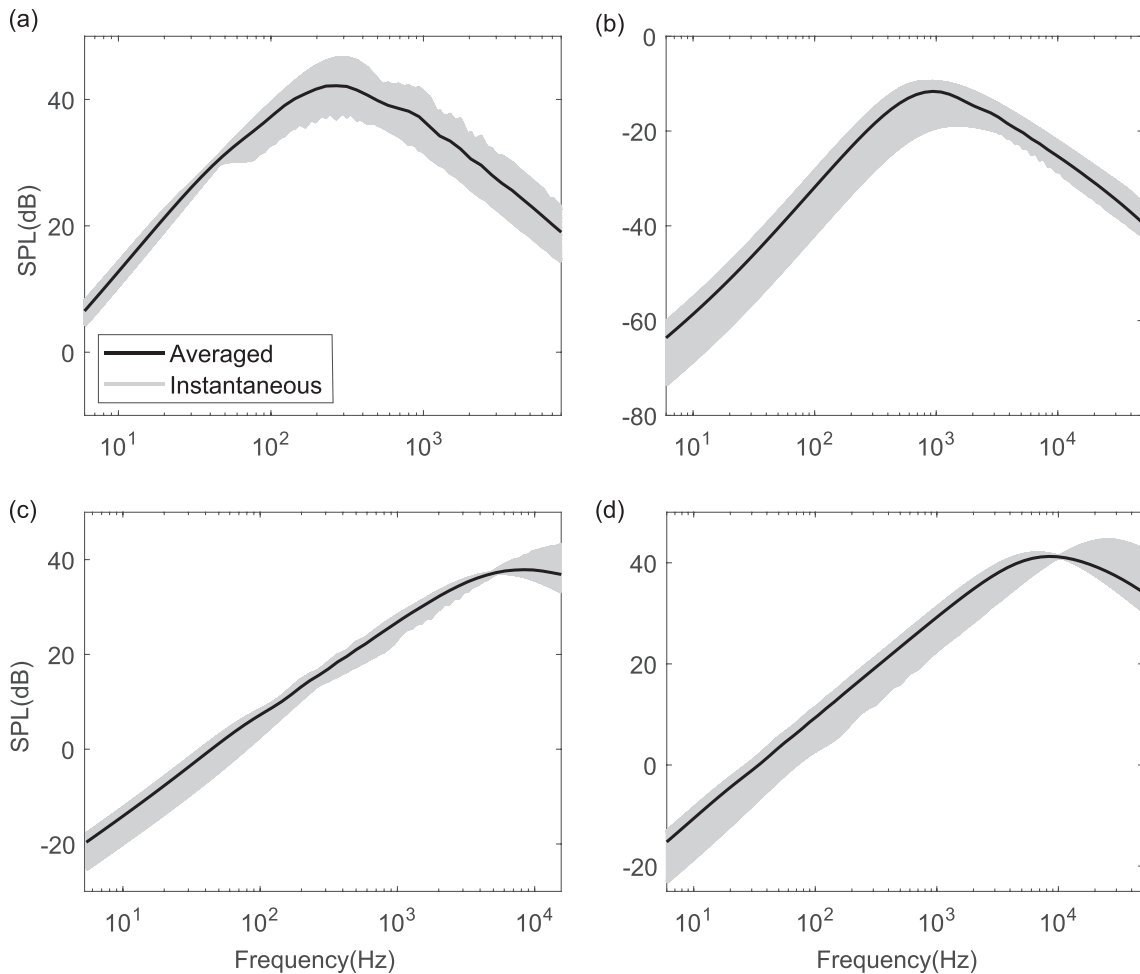


FIG. 12. Instantaneous and averaged noise spectra for rotating blade elements with straight trailing edges. (a) Wind turbine, (b) cooling fan, (c) open propeller at takeoff, and (d) open propeller at cruise.

The reason for this is that the use of serrations may lead to a significant change in the directivity pattern of an isolated flat plate. The instantaneous SPLs, therefore, obtain significantly different values as the blade rotates to different angles.

As shown in Figs. 9 and 10, there exist several peaks in the directivity patterns of the three applications at high frequency ($k_c = 50$). We attempt to explain the occurrence of those peaks. Here, the cooling fan and open propeller at cruise are selected as two examples because they represent the low and high Mach numbers, respectively. By investigating these two examples, we can identify when and why these peaks occur in Figs. 9 and 10 and get a better understanding of the effects of rotation. To do this, we need to show the instantaneous directivity perceived at a fixed rotation angle γ .

Figure 14 shows the instantaneous directivities for rotating blade elements of the cooling fan at the normalized frequency $k_c = 50$. The directivity patterns at seven rotation angles from 0° to 180° are presented with an interval of 30° . The directivity patterns at rotation angles $\gamma = 210^\circ, 240^\circ, 270^\circ, 300^\circ$, and 330° are same as that at $\gamma = 150^\circ, 120^\circ, 90^\circ, 60^\circ$, and 30° , respectively. It can be seen from

Fig. 14(a) that, for the serrated trailing edge, there is a peak at the observer angle $\theta = 30^\circ$ when the blade element is at the initial position ($\gamma = 0^\circ$). When the blade element moves to $\gamma = 30^\circ$, the position of this peak hardly moves. At the rotation angle $\gamma = 60^\circ$, the peak's position is approximately at $\theta = 45^\circ$ [Fig. 14(c)]. When the blade element moves to $\gamma = 90^\circ$, there exist no apparent peaks in the directivity pattern. As the rotation angle further increases, the peak appears again, as shown in Fig. 14(e). When the blade rotates to $\gamma = 150^\circ$ and 180° , as shown in Figs. 14(f) and 14(g), respectively, the directivity peak remains roughly at the same angle. For the open propeller, the directivity patterns are very similar to those shown in Fig. 14, which can be used to explain the appearance of the directivity peaks shown in Fig. 10. Due to their similarity, we, therefore, omit a repetitive description.

To understand the variations of the directivity as the blade rotates to different rotation angles, we draw the three-dimensional far-field noise directivity contours of an isolated flat plate with serrated trailing edges. Figure 15 presents the directivity on the side of $Z > 0$ at $k_c = 50$. The observer distance is also rescaled to 1 m. We first focus on the blade element of the cooling fan, for which the Doppler effect is weak

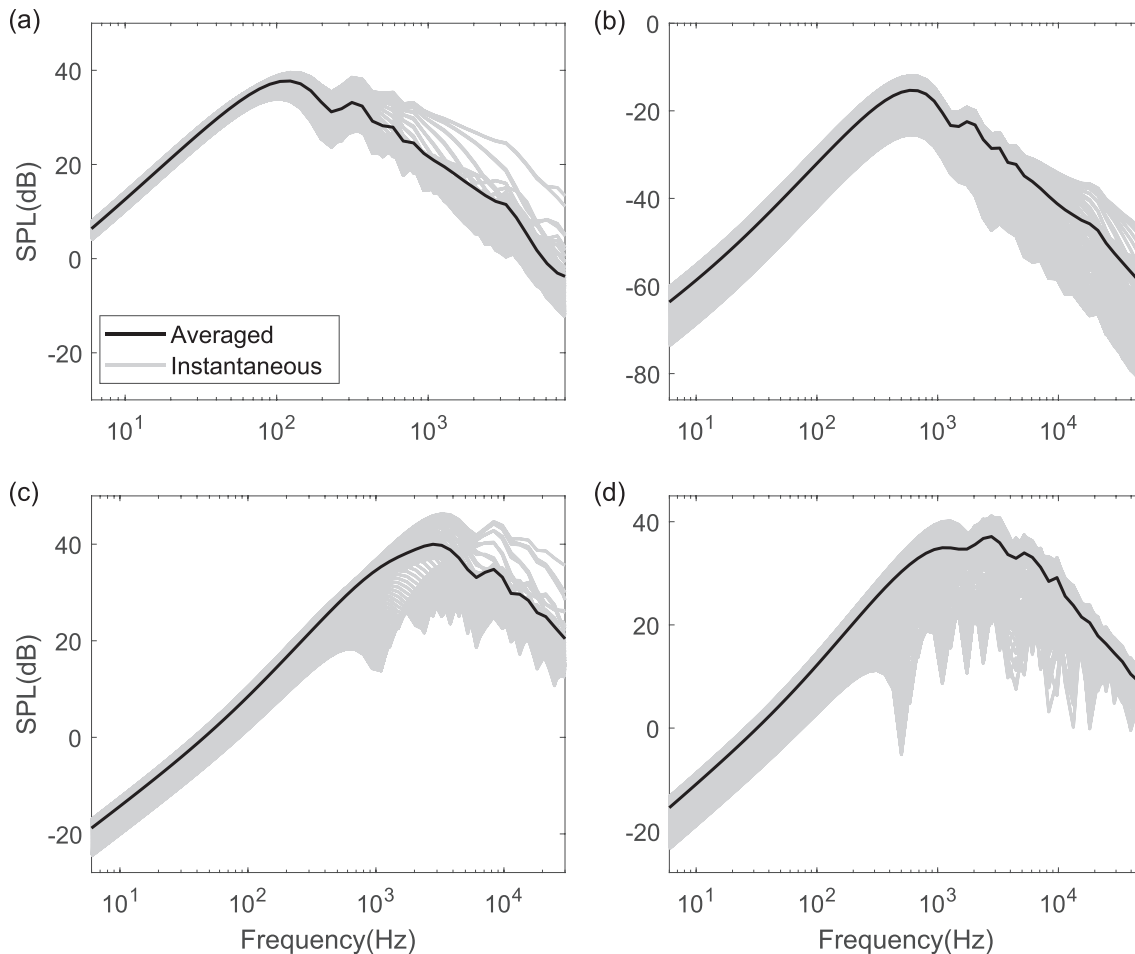


FIG. 13. Instantaneous and averaged noise spectra for rotating blade elements with serrated trailing edges. (a) Wind turbine, (b) cooling fan, (c) open propeller at takeoff, and (d) open propeller at cruise.

due to the low Mach number, and hence the perceived sound frequency is close to the emission frequency. It can be seen from Fig. 15(a) that there is an obvious peak near $X=0$. In addition, owing to the small Mach number, the present source position \mathbf{x}_p in the coordinate transformation process is close to the origin of the coordinate frame fixed to the observer. When the blade rotates to a fixed angle γ , the instantaneous directivity pattern as the observer moves from $\theta = 0^\circ$ to $\theta = 180^\circ$ in the x - z plane (see Fig. 6) is approximately identical to the pattern obtained by cutting Fig. 15(a) at a corresponding angle. For example, if the observer trajectory after coordinate transformation is in the X - Z plane (such as when $\gamma = 0^\circ$), the peak would appear at 90° in the transformed frame (corresponding to approximately 30° in the original frame because of the pitch angle of the blade). When the rotation angle equals to 90° , it can be seen from Fig. 6 that the observer's trajectory is located in the Y - Z plane. Consequently, as shown in Fig. 14(d), there exists no apparent peak in the directivity pattern. This explains why the directivity peaks occur at some rotation angles, but not at others.

We may also explain why the directivity peak angles shown in Fig. 14 remain roughly the same when the rotation angle γ is close to

0° and 180° . We see from Fig. 15 that a directivity peak always appears when the transformed coordinate X is approximately equal to 0. From the coordinate transformation [Eqs. (9)–(11)], if we set the X -coordinate to be zero and assume that the present source position is a zero vector, the relationship between the peak angle θ_p and rotation angle γ is approximately given by

$$\theta_p = \arctan\left(\frac{\tan \alpha}{\cos \gamma}\right). \quad (19)$$

Equation (19) provides an estimated explicit relation between the directivity peak angle and the instantaneous rotation angle γ .

Figure 16 shows the variation of the peak directivity angle θ_p with the rotation angle γ based on Eq. (19). It can be seen that when the blade element is located at the initial position ($\gamma = 0^\circ$), the peak angle approximately equals to the pitch angle of the blade element and is, therefore, close to 30° , as shown in Fig. 14(a). It is also clear that in the vicinity of $\gamma = 0^\circ$ and $\gamma = 180^\circ$, the variation of the peak angle θ_p is slow. This trend is in agreement with the observed results in Fig. 14.

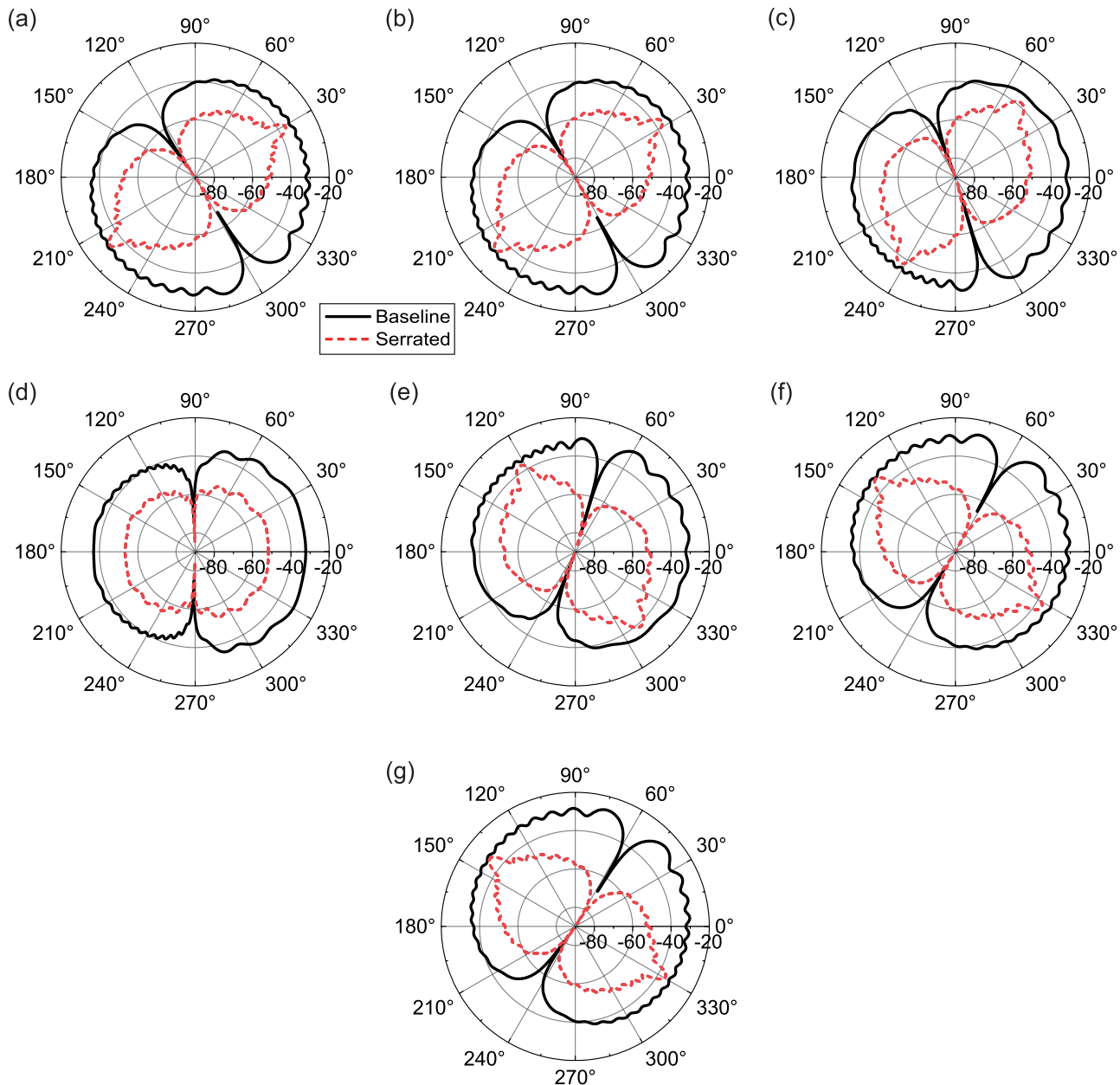


FIG. 14. Instantaneous directivities for a cooling fan blade element at various rotation angles: (a) $\gamma = 0^\circ$, (b) $\gamma = 30^\circ$, (c) $\gamma = 60^\circ$, (d) $\gamma = 90^\circ$, (e) $\gamma = 120^\circ$, (f) $\gamma = 150^\circ$, and (g) $\gamma = 180^\circ$.

Since the far-field sound pressure for a rotating blade element is an averaged result over the angular position, we can expect the peaks to appear at around $\theta = 30^\circ$ and $\theta = 140^\circ$ in Fig. 9(f). This is because as γ varies, these peak angles hardly change, therefore, resulting in a large integral value.

For open propellers at cruise, however, the Mach number is close to 1. Hence, we can expect that, as the blade rotates to different angles, the instantaneously perceived SPLs can vary significantly due to the

Doppler effect. In addition, the instantaneous directivity patterns vary in a similar manner as in the cooling fans case. Therefore, the final directivity patterns are determined by the combined contribution from the Doppler effect and the nonuniform directivity of an isolated flat plate.

The serration shape used in the present study is sawtooth and the root-to-tip amplitude and wavelength of the serration remain unchanged, i.e., the effects of serration profiles on noise reduction are

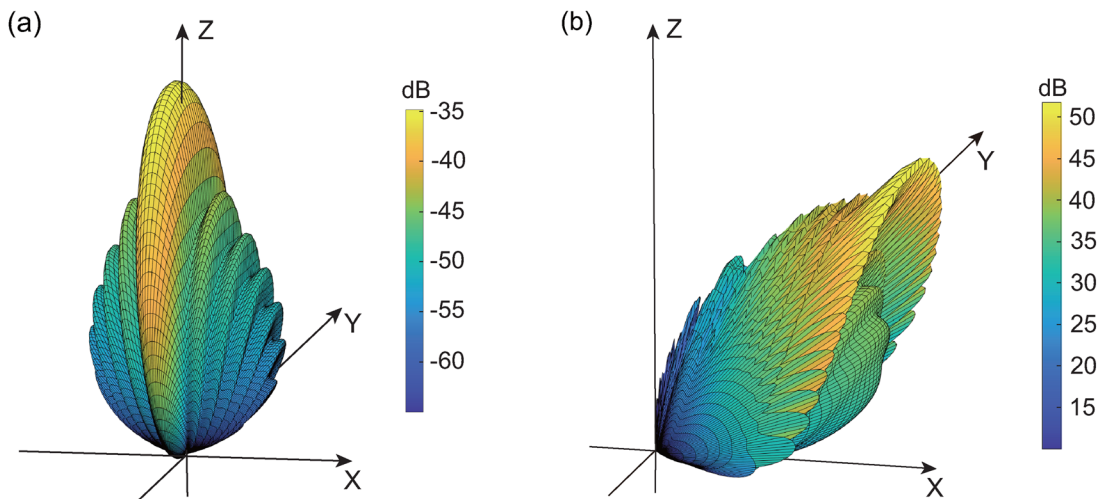


FIG. 15. Far-field SPL contours for an isolated flat plate with the serrated trailing edge. (a) cooling fan, $kc = 50$ and (b) open propeller at cruise, $kc = 50$.

not investigated here. However, from the above analysis, it can be found that the effects of rotation on the noise reduction using trailing-edge serrations are mainly due to a Doppler-weighted averaging. It can be expected that the serration profiles that lead to better noise reduction for isolated blades may also result in greater noise reduction for rotating blades, especially at low Mach numbers.

E. Discussion on the wavenumber–frequency spectrum

The wavenumber–frequency spectrum of the pressure fluctuations within the turbulent boundary layer near the trailing edge is an important input to the noise prediction model. Due to the inherent difficulty of measuring such data in experiments, empirical models are widely used in the theoretical predictions of trailing-edge noise. This paper employs Chase's model for illustration purpose, but it is useful to examine the effects of using different models. Figure 17 shows the

noise reduction spectrum using Chase's, Chou and George's, and Willmarth–Roos–Amiet models for the cooling fan case at an observer angle of $\theta = 45^\circ$. It can be seen that different models yield similar predictions. In particular, the predicted noise reduction spectra totally collapse for frequencies below 1 kHz. Difference starts to appear at high frequencies. However, as can be seen from Fig. 17, the maximum difference is around 2 dB. This suggests that the effects of rotation on the noise reduction characteristics are consistent when different spectra are used.

Using an accurate wavenumber–frequency spectrum is vital for an accurate noise prediction. Semi-empirical models based on the Reynolds-Averaged Navier-Stokes (RANS) simulations, such as the TNO-Blake model, are likely to be more reliable when realistic flow conditions are taken into consideration.^{53,54} However, it is worth noting that the present model developed in this paper is independent of the

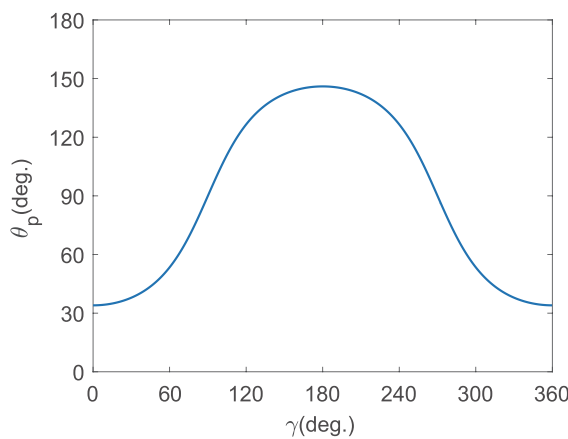


FIG. 16. Estimated relationship between the peak angle and the rotation angle.

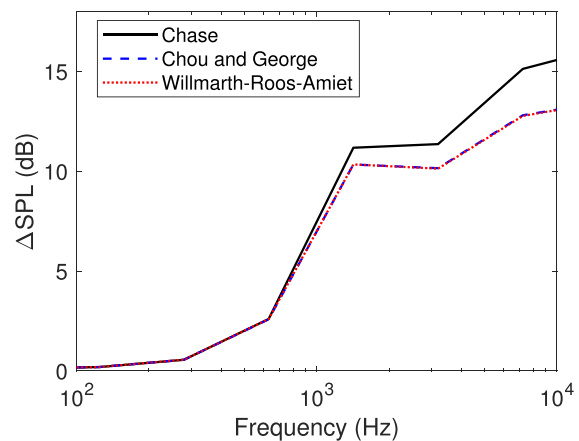


FIG. 17. Comparison of predicted noise reduction using different turbulent boundary layer models.

wavenumber-frequency spectrum and provide a more accurate spectrum, an improved noise prediction can be expected from the model. In addition, frozen-turbulence is a common assumption in trailing-edge noise problems. However, to what extent that the serrations change the flow is still open to some debate.^{29,30} The understanding of how the serration affect the flow field near the serration is another way of improving the accuracy of the model. This will be studied in our future work.

IV. CONCLUSION

In this paper, the semi-analytical noise prediction model for an isolated flat plate with serrated trailing edges developed by Lyu *et al.*¹⁸ is extended to the rotating blade using the Schlinker and Amiet's approach.⁶ The performance of solutions of various orders, the directivity patterns, and the effects of rotation are studied by applying the model to three applications including wind turbines, cooling fans, and open propellers (both takeoff and cruise conditions). These applications represent typical practical applications where trailing-edge noise can become an issue.

The model starts with an outline of the noise prediction for an isolated flat plate where the PSD of far-field noise can be calculated from the wavenumber spectral density of the wall pressure near the trailing edge. A blade segment is approximated to be tangent translating, to which the flat plate theory can be applied. To extend the model to the rotating case, the coordinate transformation from observer-fixed frame to blade-fixed frame is made. With Doppler effect taken into account, the instantaneous power spectra are averaged over rotation angle to obtain the far-field PSD of a rotating blade element. When the serration amplitude reduces to zero, the present model exhibits excellent agreement with that presented in the studies of Sinayoko *et al.*⁹

The noise spectra obtained using different-order approximations show that the second-order solution yields a converged result. The use of trailing-edge serrations results in significant noise reduction in the range of intermediate and high frequencies for the blade element of wind turbines and cooling fans. Due to the potentially constructive net effect of phase interference in high Mach numbers, noise increases are observed in intermediate-frequency range for open propellers at take-off and cruise. The noise reduction effects at different observer angles are shown in the directivity patterns at three normalized frequencies. The directivities were not studied in previous prediction models of rotating blades with serrated trailing edges and are, therefore, particularly considered in the present paper. The results show that the serrations can lead to noise reduction or increase at different observer angles for different applications. For wind turbines and cooling fans, the Doppler shift (ω/ω') is close to 1 within one rotation cycle. For open propellers, however, the Mach number is high and the Doppler effects are, therefore, significant.

The instantaneous noise spectra show that at an observer angle of 45°, the variations for serrated trailing edges are larger than that for straight ones at high frequencies. Directivity peaks are observed in all the applications at high frequencies. It is shown that for low-Mach number applications, the Doppler effect is weak and the final directivity patterns are mainly affected by the nonuniform directivity of an isolated flat plate. On the other hand, for high-Mach number applications, the final directivity patterns are determined by combined contribution from the Doppler effect and the nonuniform directivity of an isolated flat plate.

ACKNOWLEDGMENTS

The authors gratefully acknowledge the financial support from the Marine S&T Fund of Shandong Province for Pilot National Laboratory for Marine Science and Technology (Qiangdao) (No. 2022QNLM010201).

AUTHOR DECLARATIONS

Conflict of Interest

The authors have no conflicts to disclose.

Author Contributions

Haopeng Tian: Formal analysis (equal); Investigation (equal); Methodology (equal); Writing – original draft (equal). **Benshuai Lyu:** Funding acquisition (equal); Resources (equal); Supervision (lead); Writing – review and editing (equal).

DATA AVAILABILITY

The data that support the findings of this study are available from the corresponding author upon reasonable request.

APPENDIX A: COORDINATE TRANSFORM MATRICES

$$A_1 = \begin{pmatrix} \cos \gamma & \sin \gamma & 0 \\ -\sin \gamma & \cos \gamma & 0 \\ 0 & 0 & 1 \end{pmatrix}, \quad A_2 = \begin{pmatrix} \cos \alpha & 0 & -\sin \alpha \\ 0 & 1 & 0 \\ \sin \alpha & 0 & \cos \alpha \end{pmatrix}. \quad (A1)$$

APPENDIX B: AMIET'S FLAT PLATE THEORY AND SURFACE PRESSURE POWER SPECTRAL DENSITY

According to Amiet,^{4,55} for an observer at the position $\mathbf{X}_0 = (X_0, Y_0, Z_0)$, the sound PSD at frequency ω is given by

$$S_{pp}(\mathbf{X}_0, \omega) = \left(\frac{\omega Z_0 c}{4\pi c_0 S_0^2} \right)^2 \frac{d}{2} l_s(\omega, k_s) |\Psi|^2 S_{qq}(\omega). \quad (B1)$$

The spanwise correlation length and the acoustic lift can be expressed as

$$l_s(\omega, k_2) = \frac{U_c}{\omega} \frac{\eta}{\eta^2 + (U_c k_2 / \omega)^2} \quad (B2)$$

and

$$\Psi = \frac{i}{A} \left\{ \frac{\sqrt{iB}}{\sqrt{iB - iA}} \text{erf}(\sqrt{2(iB - iA)}) + e^{i2A} [1 - \text{erf}(\sqrt{2iB})] \right\}, \quad (B3)$$

where $U_c = 0.8M_0c_0$, $k_s = \frac{\omega Y_0}{c_0 S_0}$, $k_C = \frac{\omega}{c_0 \beta^2} \left(M_0 - \frac{X_0}{S_0} \right)$, $A = (\omega/U_c + k_C)/2$, $B = (\omega/U_c + \kappa + M_0\mu)c/2$, and $\mu = \frac{\omega}{c_0 \beta^2}$. η is the exponential decay rate of the spanwise coherence function and is set to 0.62. The wavenumber κ is defined as

$$\kappa \equiv \begin{cases} \mu \sqrt{1 - \frac{k_s^2}{(\beta\mu)^2}}, & k_s^2 < (\beta\mu)^2, \\ -i|\mu| \sqrt{\frac{k_s^2}{(\beta\mu)^2} - 1}, & k_s^2 \geq (\beta\mu)^2. \end{cases} \quad (B4)$$

Chou and George's model is used in the validation, which is given by

$$S_{qq}(\omega) = \left(\frac{1}{2}\rho U^2\right)^2 \frac{\delta^*}{U} F(\bar{\omega}), \quad (B5)$$

where $\bar{\omega} = \omega\delta^*/U$. The boundary layer displacement thickness δ^* at the angle of attack of χ and the function $F(\bar{\omega})$ are given, respectively, by

$$\delta^* = \begin{cases} c(24.3 + 0.6625\chi)10^{-4}, & \chi \leq 4^\circ, \\ c(26.95 + 0.6625(\chi - 4) + 0.3044(\chi - 4)^2 + 0.0104(\chi - 4)^3)10^{-4}, & \chi > 4^\circ, \end{cases} \quad (B6)$$

$$F(\bar{\omega}) = \begin{cases} \frac{1.732 \times 10^{-3}\bar{\omega}}{1 - 5.489\bar{\omega} + 36.74\bar{\omega}^2 + 0.1505\bar{\omega}^5}, & \bar{\omega} < 0.06, \\ \frac{1.4216 \times 10^{-3}\bar{\omega}}{0.3261 + 4.1837\bar{\omega} + 22.818\bar{\omega}^2 + 0.0013\bar{\omega}^3 + 0.0028\bar{\omega}^5}, & \bar{\omega} \geq 0.06. \end{cases} \quad (B7)$$

With the measurements of Willmarth and Roos,⁵⁶ Amiet proposed an surface pressure spectrum model

$$S_{qq}(\omega) = \left(\frac{1}{2}\rho U^2\right)^2 \frac{\delta^*}{U} G(\bar{\omega}), \quad (B8)$$

where $G(\bar{\omega})$ is given by

$$G(\bar{\omega}) = \frac{2 \times 10^{-5}}{1 + \bar{\omega} + 0.217\bar{\omega}^2 + 0.00562\bar{\omega}^4}, \quad 0.1 < \bar{\omega} < 20. \quad (B9)$$

The relation between the wavenumber spectrum and spanwise correlation length is¹⁰

$$\Pi(\omega, k_2) = \frac{1}{\pi} l_S(\omega, k_2) S_{qq}(\omega). \quad (B10)$$

REFERENCES

- ¹T. F. Brooks, D. S. Pope, and M. A. Marcolini, "Airfoil self-noise and prediction," NASA Report No. 1218 (1989).
- ²S. Oerlemans, M. Fisher, T. Maeder, and K. Kögler, "Reduction of wind turbine noise using optimized airfoils and trailing-edge serrations," *AIAA J.* **47**, 1470–1481 (2009).
- ³L. Chen, T. Batty, M. Giacobello, and R. Widjaja, "Prediction of small-scale rotor noise using a low-fidelity model-based framework," in *Proceedings of Acoustics* (Australian Acoustical Society, 2019), Vol. 10.
- ⁴R. K. Amiet, "Noise due to turbulent flow past a trailing edge," *J. Sound Vib.* **47**, 387–393 (1976).
- ⁵R. K. Amiet, "Noise produced by turbulent flow into a propeller or helicopter rotor," *AIAA J.* **15**, 307–308 (1977).
- ⁶R. H. Schlinker and R. K. Amiet, "Helicopter rotor trailing edge noise," NASA Report No. 3470 (1981).
- ⁷V. P. Blandeau and P. F. Joseph, "Validity of Amiet's model for propeller trailing-edge noise," *AIAA J.* **49**, 1057–1066 (2011).
- ⁸Y. Rozenberg, M. Roger, and S. Moreau, "Rotating blade trailing-edge noise: Experimental validation of analytical model," *AIAA J.* **48**, 951–962 (2010).
- ⁹S. Sinayoko, M. Kingan, and A. Agarwal, "Trailing edge noise theory for rotating blades in uniform flow," *Proc. R. Soc. A* **469**, 20130065 (2013).
- ¹⁰M. Roger and S. Moreau, "Back-scattering correction and further extensions of Amiet's trailing-edge noise model. Part 1: Theory," *J. Sound Vib.* **286**, 477–506 (2005).
- ¹¹R. R. Graham, "The silent flight of owls," *Aeronaut. J.* **38**, 837–843 (1934).
- ¹²J. W. Jaworski and N. Peake, "Aeroacoustics of silent owl flight," *Annu. Rev. Fluid Mech.* **52**, 395–420 (2020).
- ¹³P. Zhou, S. Zhong, X. Li, Y. Li, W. Chen, H. Jiang, and X. Zhang, "Broadband trailing edge noise reduction through porous velvet-coated serrations," *Phys. Fluids* **34**, 057112 (2022).
- ¹⁴X. Ji, L. Wang, S. Ravi, F.-B. Tian, J. Young, and J. C. Lai, "Influences of serrated trailing edge on the aerodynamic and aeroacoustic performance of a flapping wing during hovering flight," *Phys. Fluids* **34**, 011902 (2022).
- ¹⁵M. S. Howe, "Aerodynamic noise of a serrated trailing edge," *J. Fluid Struct.* **5**, 33–45 (1991).
- ¹⁶M. S. Howe, "Noise produced by a sawtooth trailing edge," *J. Acoust. Soc. Am.* **90**, 482–487 (1991).
- ¹⁷M. Gruber, "Airfoil noise reduction by edge treatments," Ph.D. thesis (University of Southampton, 2012).
- ¹⁸B. Lyu, M. Azarpeyvand, and S. Sinayoko, "Prediction of noise from serrated trailing edges," *J. Fluid Mech.* **793**, 556–588 (2016).
- ¹⁹X. Huang, "Theoretical model of acoustic scattering from a flat plate with serrations," *J. Fluid Mech.* **819**, 228–257 (2017).
- ²⁰L. Ayton, "Analytic solution for aerodynamic noise generated by plates with spanwise-varying trailing edges," *J. Fluid Mech.* **849**, 448–466 (2018).
- ²¹L. Jones and R. Sandberg, "Numerical investigation of airfoil self-noise reduction by addition of trailing-edge serrations," in *16th AIAA/CEAS Aeroacoustics Conference* (American Institute of Aeronautics and Astronautics, 2010).
- ²²L. E. Jones and R. D. Sandberg, "Acoustic and hydrodynamic analysis of the flow around an aerofoil with trailing-edge serrations," *J. Fluid Mech.* **706**, 295–322 (2012).
- ²³R. Arina, R. Della Ratta Rinaldi, A. Iob, and D. Torzo, "Numerical study of self-noise produced by an airfoil with trailing-edge serrations," in *18th AIAA/CEAS Aeroacoustics Conference* (American Institute of Aeronautics and Astronautics, 2012).
- ²⁴M. Sanjosé, C. Méon, M. Vianney, and S. Moreau, "Direct numerical simulation of acoustic reduction using serrated trailing-edge on an isolated airfoil," in *20th AIAA/CEAS Aeroacoustics Conference* (American Institute of Aeronautics and Astronautics, 2014).
- ²⁵T. P. Chong and A. Vathylakis, "On the aeroacoustic and flow structures developed on a flat plate with a serrated sawtooth trailing edge," *J. Sound Vib.* **354**, 65–90 (2015).
- ²⁶D. J. Moreau and C. J. Doolan, "Noise-reduction mechanism of a flat-plate serrated trailing edge," *AIAA J.* **51**, 2513–2522 (2013).
- ²⁷C. A. León, R. Merino-Martínez, D. Ragni, F. Avallone, F. Scarano, S. Pröbsting, M. Snellen, D. G. Simons, and J. Madsen, "Effect of trailing edge serration-flow misalignment on airfoil noise emissions," *J. Sound Vib.* **405**, 19–33 (2017).
- ²⁸A. Celik, Y. Mayer, and M. Azarpeyvand, "On the aeroacoustic characterization of a robust trailing-edge serration," *Phys. Fluids* **33**, 075120 (2021).
- ²⁹P. Zhou, Q. Liu, S. Zhong, Y. Fang, and X. Zhang, "A study of the effect of serration shape and flexibility on trailing edge noise," *Phys. Fluids* **32**, 127114 (2020).
- ³⁰F. Avallone, S. Pröbsting, and D. Ragni, "Three-dimensional flow field over a trailing-edge serration and implications on broadband noise," *Phys. Fluids* **28**, 117101 (2016).
- ³¹S. Lee, L. Ayton, F. Bertagnolio, S. Moreau, T. P. Chong, and P. Joseph, "Turbulent boundary layer trailing-edge noise: Theory, computation, experiment, and application," *Prog. Aerosp. Sci.* **126**, 100737 (2021).
- ³²A. Cambray, E. Pang, D. Rezgui, M. Azarpeyvand, and S. A. Showkat Ali, "Investigation towards a better understanding of noise generation from UAV

- propellers,” in *24th AIAA/CEAS Aeroacoustics Conference* (American Institute of Aeronautics and Astronautics, 2018).
- ³³P. Candeloro, R. E. Nargi, F. Patané, and T. Pagliaroli, “Experimental analysis of small-scale rotors with serrated trailing edge for quiet drone propulsion,” *J. Phys.: Conf. Ser.* **1589**, 012007 (2020).
- ³⁴T. Lan, G. Li, and M. Zhang, “Calculation method of aerodynamic performance of small propeller with serrated trailing edge,” *J. Phys. Conf. Ser.* **1600**, 012012 (2020).
- ³⁵H. M. Lee, Z. Lu, K. M. Lim, J. Xie, and H. P. Lee, “Quieter propeller with serrated trailing edge,” *Appl. Acoust.* **146**, 227–236 (2019).
- ³⁶K. D. Munz and V. Raghav, “Design and development of a small-scale coaxial rotor for aeroacoustic investigation,” in *AIAA Scitech 2020 Forum* (AIAA, 2020), p. 1497.
- ³⁷Z. Ning, R. W. Wlezien, and H. Hu, “An experimental study on small UAV propellers with serrated trailing edges,” in *47th AIAA Fluid Dynamics Conference* (American Institute of Aeronautics and Astronautics, 2017).
- ³⁸T. Pagliaroli, R. Camussi, P. Candeloro, O. Giannini, G. Bella, and R. Panciroli, “Aeroacoustic study of small scale rotors for mini drone propulsion: Serrated trailing edge effect,” in *2018 AIAA/CEAS Aeroacoustics Conference* (AIAA, 2018), p. 3449.
- ³⁹Y. Wei, Y. Qian, S. Bian, F. Xu, and D. Kong, “Experimental study of the performance of a propeller with trailing-edge serrations,” *Acoust. Aust.* **49**, 305–316 (2021).
- ⁴⁰Y. Yang, Y. Wang, Y. Liu, H. Hu, and Z. Li, “Noise reduction and aerodynamics of isolated multi-copter rotors with serrated trailing edges during forward flight,” *J. Sound Vib.* **489**, 115688 (2020).
- ⁴¹S. Sinayoko, M. Azarpeyvand, and B. Lyu, “Trailing edge noise prediction for rotating serrated blades,” in *20th AIAA/CEAS Aeroacoustics Conference* (American Institute of Aeronautics and Astronautics, 2014).
- ⁴²A. Halimi, B. G. Marinus, and S. Larbi, “Analytical prediction of broadband noise from mini-RPA propellers with serrated edges,” *Int. J. Aeroacoust.* **18**, 517–535 (2019).
- ⁴³B. Lyu and L. J. Ayton, “Rapid noise prediction models for serrated leading and trailing edges,” *J. Sound Vib.* **469**, 115136 (2020).
- ⁴⁴R. K. Amiet, “Frame of reference considerations for the forward flight noise problem,” UARL Report No. N212775-1 (1974).
- ⁴⁵S. T. Chou and A. R. George, “Effect of angle of attack on rotor trailing-edge noise,” *AIAA J.* **22**, 1821–1823 (1984).
- ⁴⁶D. M. Chase, “The character of the turbulent wall pressure spectrum at subconvective wavenumbers and a suggested comprehensive model,” *J. Sound Vib.* **112**, 125–147 (1987).
- ⁴⁷E. R. Eckert and R. M. Drake, *Heat and Mass Transfer* (McGraw-Hill, 1959).
- ⁴⁸Y. Li, Y. Yang, Y. Liu, Y. Wang, B. Huang, and W. Li, “Aerodynamic and aero-acoustic analyses of a UAV propeller with trailing edge serrations,” in *Proceedings of Acoustics* (Australian Acoustical Society, 2018), Vol. 7.
- ⁴⁹J. Mathew, A. Singh, J. Madsen, and C. A. León, “Serration design methodology for wind turbine noise reduction,” *J. Phys.* **753**, 022019 (2016).
- ⁵⁰K. Braun, N. Van der Borg, A. Dassen, F. Doorenspleet, A. Gordner, J. Ocker, and R. Parchen, “Serrated trailing edge noise (STENO),” in *European Wind Energy Conference* (James and James Science, 1999), p. 180.
- ⁵¹S. Lee and S. Lee, “Wind turbine noise reduction by means of serrated trailing edges,” in *INTER-NOISE and NOISE-CON Congress and Conference Proceedings* (Institute of Noise Control Engineering, 2012), Vol. 9, pp. 2283–2288.
- ⁵²S. Oerlemans, “Reduction of wind turbine noise using blade trailing edge devices,” in *22nd AIAA/CEAS Aeroacoustics Conference* (American Institute of Aeronautics and Astronautics, 2016).
- ⁵³Y. D. Mayer, B. Lyu, H. K. Jawahar, and M. Azarpeyvand, “A semi-analytical noise prediction model for airfoils with serrated trailing edges,” *Renewable Energy* **143**, 679–691 (2019).
- ⁵⁴O. Stalnov, P. Chaitanya, and P. F. Joseph, “Towards a non-empirical trailing edge noise prediction model,” *J. Sound Vib.* **372**, 50–68 (2016).
- ⁵⁵R. K. Amiet, “Effect of the incident surface pressure field on noise due to turbulent flow past a trailing edge,” *J. Sound Vib.* **57**, 305–306 (1978).
- ⁵⁶W. Willmarth and F. Roos, “Resolution and structure of the wall pressure field beneath a turbulent boundary layer,” *J. Fluid Mech.* **22**, 81–94 (1965).